ELSEVIER

Contents lists available at ScienceDirect

Journal of Molecular Liquids

journal homepage: www.elsevier.com/locate/molliq





Monitoring *in-situ* dissolution of polystyrene-acrylonitrile (SAN) via calorimetry and spectroscopy

Giuseppe Melilli ^a, Sandra Litwin ^a, Luc Vincent ^a, Nicolas Sbirrazzuoli ^a, Mark C.P. Roelands ^b, Jan Cornelis van der Waal ^b, Ruud Cuypers ^b, Nathanael Guigo ^{a,*}

ARTICLE INFO

Keywords:
Physical recycling
Dissolution kinetics
Polymer–solvent interactions

ABSTRACT

Dissolution/precipitation recycling is an environmentally friendly solution that could be potentially implemented for ABS recycling. In this paper, a set of useful calorimetric, spectroscopic, and rheological techniques and methods are presented to monitor *in-situ* the dissolution of the ABS matrix: poly(styrene-acrylonitrile) (SAN). In line with the Hansen solubility parameters, methyl ethyl ketone (MEK) has been selected to be a suitable solvent for SAN dissolution. Thermodynamic and kinetic aspects of the dissolution process were investigated by using calorimetry and *in-situ* ATR-FTIR spectroscopy. Through an isoconversional method, the effective activation energy and the main steps involved in the dissolution process were determined. A rheological characterization of the solution SAN-MEK was also performed to provide further information on the rheological behavior.

1. Introduction

Imagine a world without plastic sounds unrealistic today since plastic is the most widespread and used material in everyday life. The global plastic demand is expected to double before 2050 [1] which implies that the planet will hold more than 33 billion tonnes of plastic in the near future [2]. Recycling could significantly prevent the release of polymers into the environment and consequently reduce microplastic pollution. Although recycling is the more reasonable way forward, out of a total of 460 million tons of plastics produced every year only about 9 % gets recycled [3]. Inadequate post-consumer plastic disposal, costs, and technological limitations in the recycling process mainly give such low figures. As a result, only few thermoplastics are efficiently recycled including polyolefins, poly (ethylene terephthalate), and polystyrene [4].

ABS (acrylonitrile-butadiene-styrene) is a thermoplastic amorphous terpolymer well-known to be highly versatile, durable, and tailorable to a large range of applications including automotive, construction, electronics, toys, and others. From a structural point of view, ABS is composed of rubber particles, usually polybutadiene (PBR) or a butadiene copolymer, dispersed in a thermoplastic matrix of styrene and acrylonitrile copolymer (SAN). The global ABS market is expected to reach USD 46.88 Billion by 2027 [5], which means that ABS recycling

will become a necessary eco-friendly practice to minimize waste and reduce the environmental impact. Currently, there are limited technological solutions to efficiently recycling end-of-life ABS products [6]. Mechanical recycling of waste ABS is the first-choice method for closed-loop recycling in the automotive industry [7]. Nevertheless, degradation during the polymer lifetime and thermo-degradation due to the reprocessing strongly affect the number of possible recycling cycles [8].

The dissolution/precipitation technology is one type of physical recycling and an environmentally friendly approach that allows recovering polymers from the formulated plastics. The recovered polymers have a quality comparable to the virgin ones [9]. Such technology can convert ABS waste into almost pure SAN with the advantage of removing unwanted additives from the waste products [10]. Lu et al. [11], reported a dissolution/precipitation recycling process for post-consumer plastic toys. Acetone and water were selected respectively as solvent and antisolvent to recycle SAN. The solvent selection is a crucial aspect of the dissolution process. Therefore, a mixture of solvents might efficiently separate polymer blends such as polycarbonate and ABS from waste electrical and electronic equipment (WEEE) [12]. Switchable solvents were employed to separate organophosphates flame retardants from commercial PC/ABS blends. [13] In the same line, CreaSolv® were employed to remove inorganic colour pigments (titanium dioxide, chromium oxide, iron oxide) from ABS [14]. Polymer fractionation

E-mail address: Nathanael.GUIGO@univ-cotedazur.fr (N. Guigo).

a Institut de Chimie de Nice, Université Côte d'Azur, CNRS, UMR 7272, 06108 Nice, France

^b TNO, Leeghwaterstraat 44, 2628CA Delft, The Netherlands

^{*} Corresponding author.

model (PFM) based on Hansen solubility parameters (HSP) allows to identify potential 'strong' or 'weak' solvents for a given polymer [15]. Although the Hansen method is suitable for setting solvents able to dissolve polymers in chemical recycling process [16], such parameters do not give further information about the kinetic and thermodynamic driving forces.

Various phenomenological models were proposed to explain the dissolution of glassy polymers including external mass transfer, stress relaxation, Fickian equations, continuum framework, etc. [17]. To support the phenomenological models, experimental techniques were set up to monitor the dissolution process including ellipsometry [18], nuclear magnetic resonance [19], FT-IR imaging, differential refractometry, optical microscopy etc. [17]. These techniques provide mainly information about the structure of the different layers (gel, solvent, and bulk), swelling behaviour, and dissolution rate. However, an in-situ monitoring of the microscopic interaction between polymer–solvent remains a challenge.

In view of ABS recycling, we propose a new approach for monitoring the in-situ dissolution of the main ABS component: SAN. A screening of different commercial solvents was performed based on the Hansen method and boiling point. Butanone (MEK) was selected to be the most suitable solvent for this study. Calorimetric and spectroscopic analysis (ATR-FTIR) have been used to follow in-situ the dissolution process. Advanced isoconversional analysis performed under isothermal conditions reveals the main steps of dissolution and associated activation barriers. A rheological study of the SAN-MEK solutions was also conducted to complete the characterization.

2. Material and methods

2.1. Materials

SAN was supplied by Trinseo NL: density (1.08 g.mL $^{-1}$), molecular weight (M $_{\rm w}=90,000$ g.mol $^{-1}$). The glass transition temperature ($T_{\rm g}$) of SAN measured by DSC was about 105 °C. Methyl-Ethyl Ketone (MEK) was analytical grade and was purchased from Honeywell Riedel de Haën

2.2. Rheological measurements

Rheological measurements were conducted by rotational rheometer Thermo Scientific HAAKE MARS with 35 mm parallel plate geometry and 0.5 mm gap. Viscosity of SAN/MEK solution (concentration 6, 8, 10, 12, 14, 16, 18, 20, and 22 %w/v) was measured at 30 °C with a shear rate ranging from 10 to $1000~\rm s^{-1}$. Frequency sweep of SAN/MEK solution (concentration 8, 12, 18, 22 %w/v) were conducted in a range of frequency between 0.1 and 100 Hz with 25 % amplitude. The amplitude value was determined from a prior stress-sweep experiment to identify the linear viscoelastic region (LVR) profiles.

2.3. In-situ ATR-FTIR analysis

The dissolution process was investigated using *in-situ* ATR-FTIR. A Bruker TENSOR 27 spectrophotometer equipped with a diamond crystal was used in ATR mode to conduct 64 scans from 4000 to 600 cm $^{-1}$, accumulated with a resolution of 4 cm $^{-1}$. A device composed of a sealed cylindrical cell in Teflon was designed to monitor the band changes function of the temperature (30, 40, and 50 °C). The background was performed without solvent and by taking attention to place the SAN pellets (100 mg) around the diamond of ATR. MEK (0.5 mL) was injected in the cell at t = 0 min. The spectra were recorded every 2 min in a static mode. Over time, the characteristic bands associated with the SAN appeared which indicate the polymer dissolution at the given temperature. MEK was used to record blank spectra at the different temperatures (30, 40, and 50 °C). Finally, the blank spectra were subtracted to sample spectra.

2.4. Reactive calorimeter (C80)

The dissolution of the mixture SAN/MEK (concentration 20 % w/v) was monitored by using a C80 Calvet type calorimeter (Setaram). This apparatus operates with two cells symmetrically placed in a calorimetric block (sample and reference). Temperature and enthalpy calibrations were performed by using indium, and Wood's metal. The heat flow associated to the static dissolution process has been monitored at different isothermal temperature T=30, 40, 50, and 60 °C. The sample collection was recorded for 250 min (the time needed for the heat flow signal to return to the baseline). The reference cell was empty during the heat flow signal acquisition. Blank curves were recorded at the different temperature (T=30, 40, 50, and 60 °C) by using only MEK. The sample and the blank curves were then subtracted to erase the influence of the solvent.

3. Theoretical part

3.1. Hansen theory

The Hansen solubility parameter (HSP) model is based on three different types of interaction: dispersion force (δ_d) , hydrogen bonding (δ_H) , and dipole–dipole forces (δ_P) . Such parameters allow to define a 3D space characterized by a sphere. According to the model, the centre of the sphere has the HSPs of the polymer, while the radius R_0 is named the interaction radius. In the Hansen space, the "distance" R_a between polymer and solvent is evaluated as follows:

$$R_a^2 = 4(\delta_{D,p} - \delta_{D,s})^2 + (\delta_{P,p} - \delta_{P,s})^2 + (\delta_{H,p} - \delta_{H,s})^2$$
(1)

where parameters with the subscript "s" and "p" denoted the solvent and polymer, respectively. The relative energy difference (RED) defined as follows:

$$RED = \frac{R_a}{R_0} \tag{2}$$

According with this definition: RED < 1 indicates high affinity between the polymer and solvent, whereas for RED > 1 the energy difference increases leading to low affinity between the polymer and solvent. Partial dissolution is possible in boundary condition (RED = 1).

3.2. Estimation enthalpy of mixing (ΔH_{mix}) from Flory-Huggins (FH) model

According to the FH model, the free energy of mixing (ΔG_{mix}) is given by the following equation:

$$\Delta G_{mix} = kT[N_1 \ln(\varnothing_1) + N_2 \ln(\varnothing_2) + \chi_{12} N_1 \varnothing_2]$$
(3)

where k is the Boltzmann constant, T the absolute temperature in Kelvins, N_1 , and N_2 are the number of moles of solvent and polymer, ϕ_1 and ϕ_2 the volume fraction of solvent and polymer, and χ_{12} is the FH interaction parameters. In FH lattice model, each site is occupied by one molecule of solvent or by one monomer unit of the macromolecules. According to this definition the total number (N) of sites is:

$$N = N_1 + rN_2 \tag{4}$$

where r is the number of segments in the polymer chain, and it is the ratio between the molar volume of the polymer and the solvent. Thus, the volume fractions are defined as:

$$\emptyset_1 = \frac{N_1}{N_1 + rN_2} \tag{5}$$

$$\emptyset_2 = 1 - \emptyset_1 \tag{6}$$

Since the thermodynamics equation of the free energy is given by:

$$\Delta G_{mix} = \Delta H_{mix} - T \Delta S_{mix} \tag{7}$$

where ΔH_{mix} , ΔS_{mix} , are respectively the enthalpy and entropy of mixing, and T is the absolute temperature. The enthalpic and entropic terms can be extrapolated by the Eq. (3) resulting in:

$$\Delta H_{mix} = RT\chi_{12}n_1\varnothing_2 \tag{8}$$

$$\Delta S_{mix} = -R[n_1 ln \varnothing_1 + n_2 ln \varnothing_2] \tag{9}$$

with R the gas constant obtained by multiplying the Avogadro's number N_A and k. Hence, n_1 and n_2 correspond to the mole of solvent and polymer in the system.

3.3. Estimation of the Flory-Huggins interaction parameter from Hansen parameters

The FH interaction parameter for a given solvent and polymer can be estimated by using Hansen solubility parameters:

$$\chi_{12} = \beta \frac{\nu_1}{RT} \left[(\delta_{Dp} - \delta_{D,s})^2 + \frac{1}{4} (\delta_{P,p} - \delta_{P,s})^2 + \frac{1}{4} (\delta_{H,p} - \delta_{H,s})^2 \right]$$
(10)

where ν_1 is the molar volume of the solvent, R the gas constant and T the absolute temperature. Hansen parameters with the subscript "s" and "p" denoted the solvent and polymer, respectively. This equation is an extension of the Hildebrand's method which includes dipolar or hydrogen bonding interactions [20]. β is a constant and is generally equal to 1 when dispersion forces dominate over polar and hydrogen bonding [21].

3.4. Kinetics and isoconversional method

The general form of the basic rate equation to kinetic analysis of the condensed phase processes is usually written as [22]:

$$\frac{\mathrm{d}\alpha}{\mathrm{d}t} = k(T)f(\alpha) = A \exp\left(-\frac{E}{RT}\right)f(\alpha) \tag{11}$$

where α is the extent of conversion of the reactant to products, t is the time, T is the absolute temperature, k(T) is the effective rate coefficient, which is assumed to obey an Arrhenius law dependency, $f(\alpha)$ is the differential form of the mathematical function that describes the reaction model representing the reaction mechanism, E is the activation energy, E is the pre-exponential factor and E is the gas constant. A list of common reaction models is found elsewhere [23].

A key parameter to follow the course of a chemical reaction or of a physical transformation is the extent of conversion α . This parameter can easily be obtained from calorimetric data either isothermal or nonisothermal from Eq. (2):

$$\alpha_{i} = \frac{\int_{t_{1}}^{t_{i}} (dH/dt)_{i} dt}{\int_{t_{2}}^{t_{2}} (dH/dt)_{i} dt} \equiv \frac{H_{i}}{Q}$$
(12)

In this equation, $(dH/dt)_i$ represents the heat flux measured by the calorimeter at time i (t_i). t_1 and t_2 correspond respectively to the time of the first and last integration bounds of the calorimetric signal. Isoconversional method have been found to be very efficient for elucidation of complex multi-step processes [24,25,26,27].

The simplest isoconversional method is the Friedman's method represented by Eq. (13) which is obtained after linearization of Eq. (11) [28]:

$$\ln\left(\frac{\mathrm{d}\alpha}{\mathrm{d}t}\right)_{\alpha i} = \ln[A_{\alpha}f(\alpha)] - \frac{E_{\alpha}}{RT_{\alpha i}} \tag{13}$$

The subscript α indicates that the computations are performed for a constant value of α and the subscript i correspond to the i temperature program used.

The advanced non-linear isoconversional method (NLN) used in this study is based on Vyazovkin's equations [29,30,31] and is expressed by Eqs. (14) and (15) that have been derived from the basic rate Eq. (11):

$$\Phi(E_{\alpha}) = \sum_{i=1}^{n} \sum_{j\neq i}^{n} \frac{J[E_{\alpha}, T_{i}(t_{\alpha})]}{J[E_{\alpha}, T_{j}(t_{\alpha})]}$$
(14)

$$J[E_{\alpha}, T(t_{\alpha})] \equiv \int_{t_{\alpha}, t_{\alpha}}^{t_{\alpha}} \exp\left[\frac{-E_{\alpha}}{RT(t)}\right] dt$$
 (15)

where E_{α} is the effective activation energy. The E_{α} value is determined as the value that minimizes the function $\Phi(E_{\alpha})$. This non-linear kinetic method (NLN) is applied to different temperature programs $T_i(t)$ and was implemented in an internally generated software [27,32,33].

The computations yield the values of effective activation energy E_{α} as a function of extent of conversion α evaluated without assumption on the reaction mechanism. It was shown that E_{α} -dependencies allow for meaningful mechanistic analyses and for understanding multi-step processes [23,34,35].

4. Results and discussions

Suitable solvents for SAN dissolution were predicted theoretically based on the HSP model. According with Hansen [15], HSPs for SAN and a list of some good solvents are presented in Table 1. For such systems the RED has been calculated according to Eqs. (1), and (2) (Table 1).

The relative position of the HSPs of the solvents compared to the HSPs of the SAN (i.e. center of the sphere) can be visually spotted in a 3D Hansen space representation (Fig. 1).

According to Fig. 1, MEK and acetone are closer to the center of the sphere with RED respectively of 0.6, and 0.49. In addition to the relative position in the sphere, the boiling temperature has been considered for the selection of the solvent. Since kinetic and thermodynamic aspects of the dissolution will be studied in this paper, low boiling solvents are less recommended for such purposes as investigations should be done on a sufficiently large temperature range. Among the commercial solvents presented in Table 1, MEK fulfils both parameters (low RED, and relatively high boiling temperature). MEK that is boiling around 80 °C allows investigating the dissolution on a temperature range of about 60 °C.

4.1. Thermal analysis

The SAN dissolution was monitored *in-situ* by means of calorimetry. The sample cell of the instrument is vertically divided in two compartments separated by a Teflon membrane. SAN is placed on the bottom of the cell, and MEK on the top. The dissolution takes place once the separating membrane is broken, and the solvent comes in contact with SAN (schema inset of Fig. 2). Although the heat flow signal is monitored from the beginning of the experiment, the dissolution process started one minute later once the membrane was pierced. The enthalpy

Table 1HSPs and boiling point for SAN and some commercial solvents, RED evaluation according with Eqs. (1), and (2).

	Solubility parameters (MPa ^{1/2})				
	δ_d	δ_P	δ_H	RED	Boiling T (°C)
SAN	16.6	9.8	7.6	_	_
Acetone	15.5	10.4	7	0.49	56
MEK	16	9	5.1	0.60	80
Acrylonitrile	16	12.8	6.8	0.69	77
Tetrahydrofuran (THF)	16.8	5.7	8	0.86	66
Ethyl acetate	15.8	5.3	7.2	1	77
Dichloromethane (DCM)	18.2	6.3	6.1	1.04	40

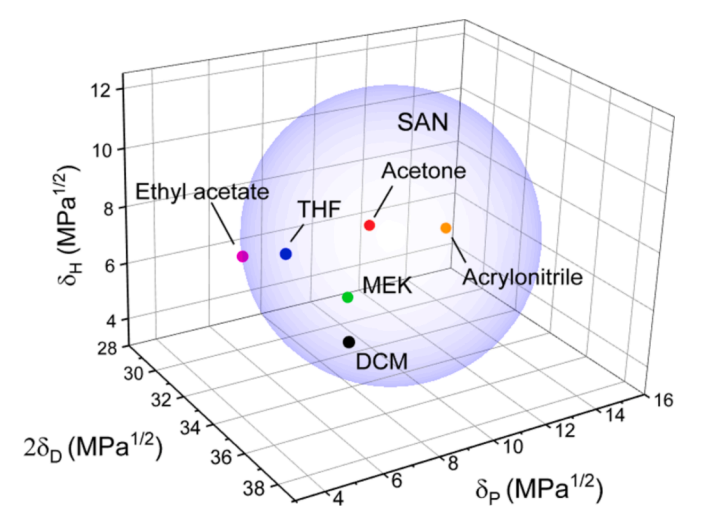


Fig. 1. Hansen solubility sphere for SAN along with some good and partially good solvents.

associated to the dissolution process is exothermic and defined as the enthalpy of dissolution (ΔH_{diss}) (Fig. 2).

 ΔH_{diss} measured at 30, 40, 50, 60 °C corresponds to 33, 30, 24, and 20.5 J.g⁻¹, respectively. Since ΔH_{diss} is an extensive function of state, it might be described by the sum of two enthalpic contributions [36,37]:

$$\Delta H_{diss} = \Delta H_{transition} + \Delta H_{mixing} \tag{16}$$

According to Eq. (16), the dissolution in glassy polymer involves two steps: firstly, a phase change of the polymer is observed from the solid to the rubbery state. The enthalpic contribution associated to this step is given by $\Delta H_{transition}$. Such enthalpy term is always exothermic because the sign of the cohesive energy in polymers is negative [38]. As the solvent interacts with the glassy polymer during dissolution, the constrained polymer chains gain flexibility. This transformation from a glassy to a more rubbery state releases excess enthalpy, resulting in heat generation and enthalpy relaxation. The enthalpic contribution related to the polymer-solvent interactions is associated to the term ΔH_{mixing} (Eq. (8)). Since the dissolution of SAN in MEK is not an ideal solution $(\Delta H_{mix} \neq 0)$, the Gibbs free energy change (ΔG_{mix}) is given by Eq. (7). Thermodynamics requires that for spontaneous dissolution of polymers, ΔG_{mix} should be negative. In dissolution process, ΔS_{mix} is positive due to an increase of the entropy of the polymer chains under the influence of the solvent. To promote dissolution ΔH_{mix} should be smaller than the term $T \Delta S_{mix}$. Strictly speaking, the mixing will be favoured when ΔH_{mix} is minimized which entails that $\delta_{D,s} \approx \delta_{D,p}$, $\delta_{P,s} \approx \delta_{P,p}$, and $\delta_{P,s} \approx \delta_{P,p}$. The estimation of ΔG_{mix} (Eq. (3)) for the system SAN/MEK shows a negative

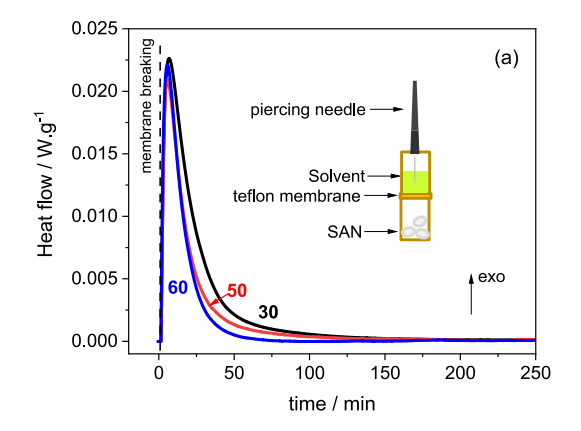
concave curve as a function of the volume fraction ϕ_2 which suggest a spontaneous process. This effect is more pronounced by increasing the temperature from 25 °C to 60 °C as shown in Fig. S1.

 χ_{12} can be calculated (Eq. (10)) by using the Hansen parameters defined at room temperature (Table 1). χ_{12} for the mixture SAN/MEK is equal to 0.077 at 25 °C. For the system SAN/MEK (concentration 20 %) the theoretical ΔH_{mix} was calculated around 1.63 J.g $^{-1}$ (per gram of polymer) (Eq. (8)), whereas the variation of ΔH_{mix} as function of ϕ_2 is presented in Fig. S2. Thus, the enthalpic contribution ΔH_{mix} is negligible in comparison with $\Delta H_{transition}$ in the measured ΔH_{diss} .

As observed in Fig. 2b, the ΔH_{diss} linearly decreases as a function of the temperature. It should be noted that ΔH_{diss} (from 20.5 to 33 J.g⁻¹) is ten to twenty times larger than the theoretical ΔH_{mix} of 1.63 J.g⁻¹. So, according to Eq. (16), the main enthalpic contribution of ΔH_{diss} is $\Delta H_{transition}$. Below the $T_{\rm g}$ of SAN (105 °C) the reduced intermolecular distance among the polymer chains prevents them to reach an equilibrium conformation. Hence, the glassy polymer possesses an excess of enthalpy due to 'frozen-in' oscillation modes. During the polymer dissolution, the frozen-in modes relaxe and $\Delta H_{transition}$ is released [38,39]. The mobility of the chains is more and more constrained with the decreasing of the temperature which suggests higher $\Delta H_{transition}$ at lower temperature [39]. If a dissolution process was theoretically performed at temperature around the T_g of the SAN (105 °C), then the $\Delta H_{transition}$ will be expected to be almost zero since the polymer molecular chains are already in their flexible state. From the linear fit in inset Fig. 2, the extrapolated value of ΔH_{diss} at 105 °C is around 1.3 J.g⁻¹. Thus, this residual enthalpy could be fairly associated to ΔH_{mix} which was theoretically calculated around 1.63 J.g⁻¹. Moreover, it can observed that the $\Delta H_{transition}$ and ΔH_{mix} are both exothermic.

According to Eq. (13), the integration of the calorimetric curves (Fig. 1) gives the relative extent of conversion (α) (Inset of Fig. 3). Generally, an overall increase in the rate of solubility/diffusion/permeation is observed by increasing the temperature.

The variation of the effective activation energy (E_{α}) was computed by using the isoconversional methods (Friedman and NLN). In Fig. 3, E_{α} is plotted as function of extent of conversion, α . A good agreement between the two methods is observed. Each E_{α} variation is associated with a change in the dissolution process. The quasi-constant value of E_{α} between 10 and 70 % indicates that the dissolution is mainly dominated by a single-step process, while the relatively low values (i.e. between 10 and 30 kJ/mol) of E_{α} indicate that the dissolution rate is mostly governed by a diffusion control. An increase of E_{α} at the end of the process was also observed. As reported earlier [40], the apparent activation energy for diffusion is larger in the rubbery state than in the glassy state. Thus, the E_{α} increase observed for $\alpha > 0.7$ is consistent with the progressive transition from a glassy to a rubbery state during dissolution.



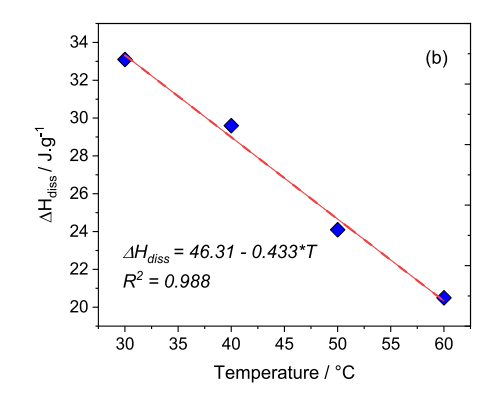


Fig. 2. (a) SAN dissolution thermograms at different temperature: black line (T = 30 °C), red line (T = 50 °C), and blue line (T = 60 °C). Inset: scheme C80 cell; $\Delta H_{\rm diss}$ versus temperature (filled blue diamond), and linear fit (dash red line).

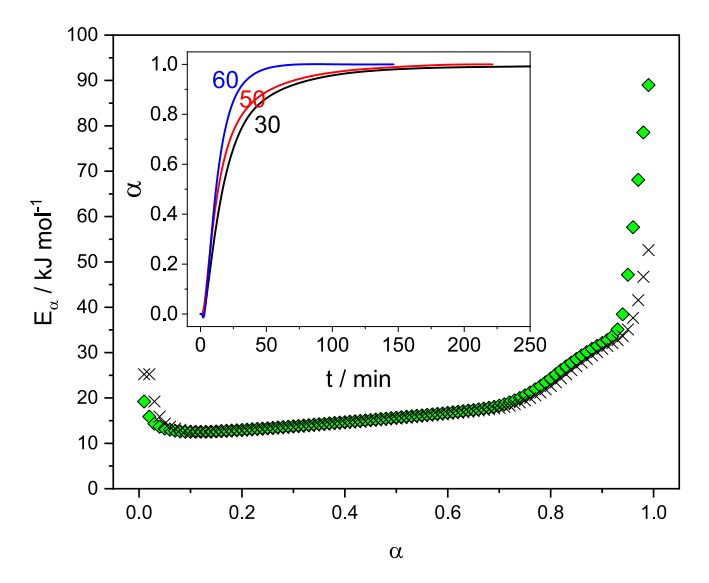


Fig. 3. Variation of the apparent activation energy (E_a) with extent conversion (α), called E_{α} -dependencies for NLN method (diamond) and Friedman method (cross). Inset: Extent conversion (α) vs. time (t) for three temperatures T=30, 50 and 60 °C.

4.2. Real-time ATR-FTIR analysis

The dissolution of SAN into MEK was monitored in real-time mode by ATR-FTIR at different temperature (i.e. 30, 40, and 50 °C). To follow up the dissolution, the intensity changes of the bands attributed to SAN were considered. The sealed device that was adapted to our ATR-FTIR is not fully hermetic so the if vapor pressure of the solvent is too high, we might consider some solvent evaporation close to the boiling point of the solvent. It explains why we have limited our experiments to a maximum temperature of 50 °C where no solvent evaporation was noticed. The bands corresponding to SAN are shown in Fig. 4. In particular, the bands at 3027, 2923, and 2855 cm⁻¹ are associated to the aromatic and aliphatic C—H stretching. The peak at 2238 cm⁻¹ is the C=N stretching in acrylonitrile. The bands peaking at 1583 and 1493 cm⁻¹ belong to the ring mode of styrene, while the scissoring mode of CH₂ in styrene is found at 1452 cm⁻¹. The bands at 702 and 755 cm⁻¹ are attributed to the C—H deformation (out-of-plane) in styrene [41,42].

The band selected for monitoring the SAN dissolution should not

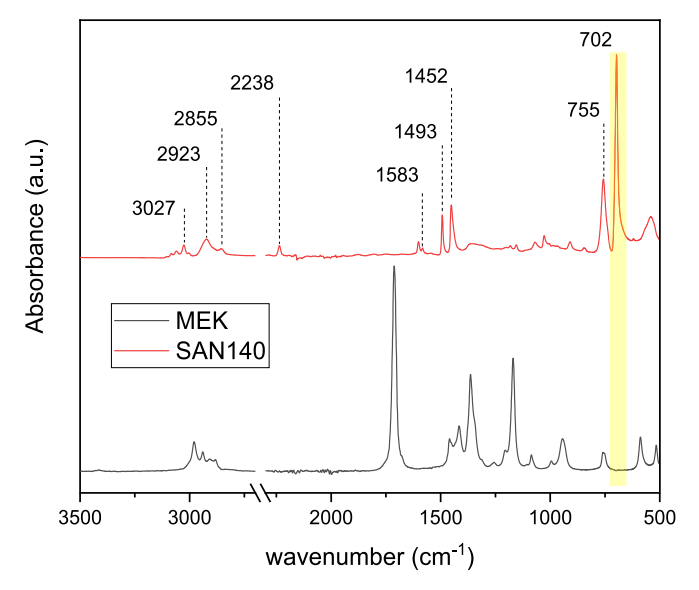


Fig. 4. ATR-FTIR spectra of SAN (red line), and MEK (black line).

overlap with the band of MEK and should be sufficiently intense. Therefore, as shown on FTIR spectra of MEK and SAN (Fig. 4), the C—H deformation (out-of-plane) band of styrene at $702~{\rm cm}^{-1}$ satisfies both conditions.

A typical evolution of the selected characteristic band during the dissolution process is shown in Fig. 5a. Similar trends were observed for the other SAN bands including 755, 2238, 1493 cm⁻¹ (data not shown). The band related to C—H deformation of the styrene moieties in the dissolved SAN appears two minutes after the beginning of the static dissolution process. This could indicate that for the mixture SAN/MEK, the swollen layer into the pellet is very thin and promptly disappears under the effect of the solvent. Similar results were reported for PAN in DMSO and DMF [43].

The normalized intensities of the band 702 cm⁻¹ are shown in Fig. 5b. The dissolution process proceeds faster by increasing the temperature from 30 to 50 °C. Furthermore, a plateau is reached after 64, 48, and 40 min respectively at 30, 40, and 50 °C. At the plateau, the formation of a compact gel layer is observed as the experiment is performed in a static mode. Moreover, the relatively large density difference between SAN (1.08 g.mL⁻¹) and MEK (0.805 g.mL⁻¹) promotes the deposition of this gel layer on the bottom of the cell thus closer to the diamond crystal in the ATR-FTIR set-up. Beyond the plateau, the intensity of the band starts decreasing over the time for all the tested temperatures. Since the band intensity change correlates with a SAN concentration change in the gel layer, the intensity decrease reflects a diffusion of the polymer chains from the gel layer into the global volume.

An extent of conversion for the gel layer formation can be estimated from the intensity curves versus time. If we consider the curves up to the plateau, then $\alpha_{FTIR} \equiv I_{702} \ (t)/I_{702} \ \text{max}$. The effective activation energy (E_{α}^{FTIR}) for the gel formation was calculated with the isoconversional method (Fig. S3). The resulting E_{α}^{FTIR} was estimated around 15 kJ.mol⁻¹ which agrees nicely with the quasi-constant value E_{α}^{C80} calculated between 10 and 70 % of conversion (Fig. S3).

As shown in Fig. 6, the conversion curves obtained by calorimetry (α_{C80}) and FTIR (α_{FTIR}) at $T=50~^{\circ}$ C are different. The α_{FTIR} reaches full conversion faster than α_{C80} (Fig. 6). The difference between calorimetry and FTIR data can be explained by the different meanings of the 'conversion'. A global conversion was measured by calorimetry whereas only a relative extent of conversion (i.e. formation of the gel layer) was obtained by using ATR-FTIR. As highlighted in Fig. 6, the full conversion ($\alpha_{FTIR}=1$) in FTIR corresponds to $\alpha_{C80}=0.86$. It is worth noting that $\alpha_{C80} = 0.86$ is associated with the increase of E_{α} values. Accordingly, the increase of E_{α} values for $\alpha_{C80} > 0.86$ can be attributed to the diffusion of SAN chains from the gel layer to the global volume of the polymer solution. This agrees well with previous works where it was shown that an increase of E_{α} is associated to a control by diffusion of long chain segments [24,34,44,45]. The rate of dissolution is then mostly controlled by the diffusion of small solvent molecules (α_{C80} < 0.86) – marked by low values of E_{α} while it becomes controlled by diffusion of long polymer chains in the being the rate-limiting step for the dissolution in this case.

The carbonyl band shift of MEK was also monitored during the dissolution of SAN (Fig. S4) at 30 $^{\circ}$ C. A redshift of the band 1712 cm $^{-1}$ was observed during dissolution compared the neat solvent at the same temperature. The shift is probably due to the formation of polar-polar interactions between the nitrile group of SAN and the carbonyl group of MEK. Similar results were reported in a solution of polyacrylonitrile in dimethyl formamide [46]. A plateau was observed after 60 min of dissolution. This agrees with the results of the intensity change shown in Fig. 5b.

4.3. Rheological measurements

The rheological behavior of the polymer solutions is essential for understanding and optimizing the solvent-based recycling processes. The viscosity as a function of the shear rate was measured for different

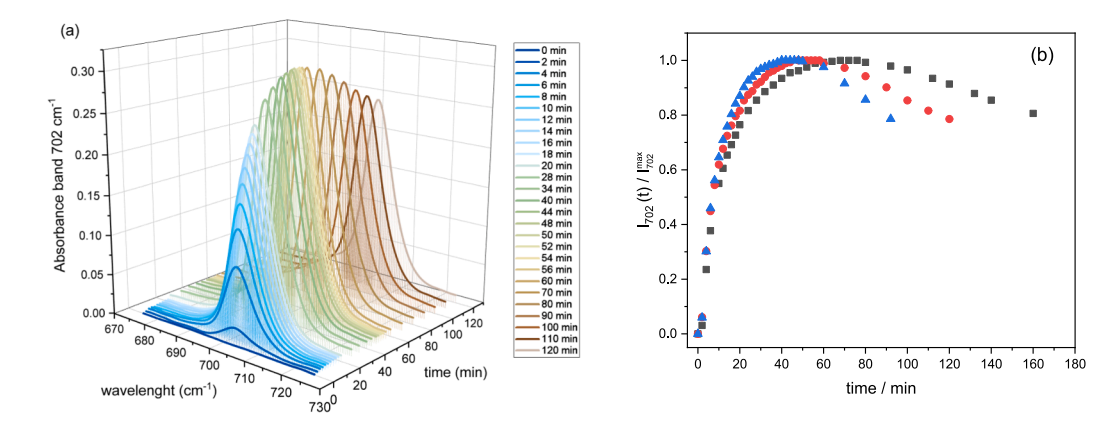


Fig. 5. (a) 702 cm⁻¹ band evolution versus time at T = 40 °C; normalized intensity variation versus time at different temperatures: T = 30 °C (filled black square), T = 40 °C (filled red circle), and T = 50 °C (filled blue triangles).

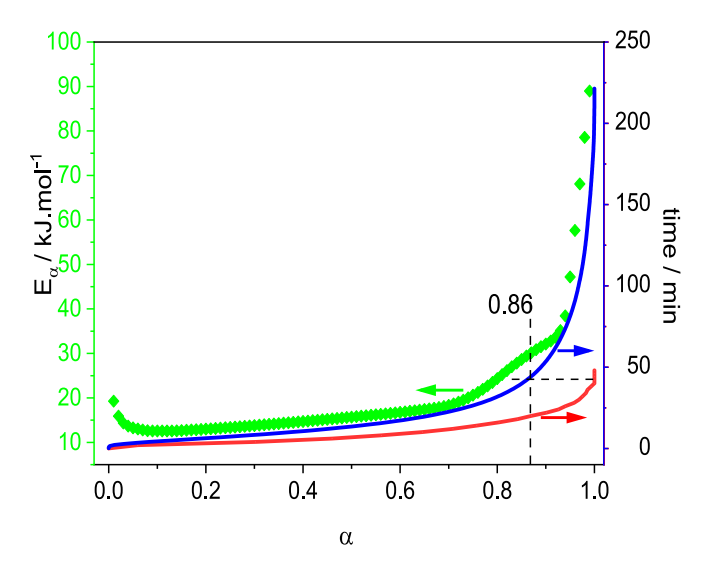


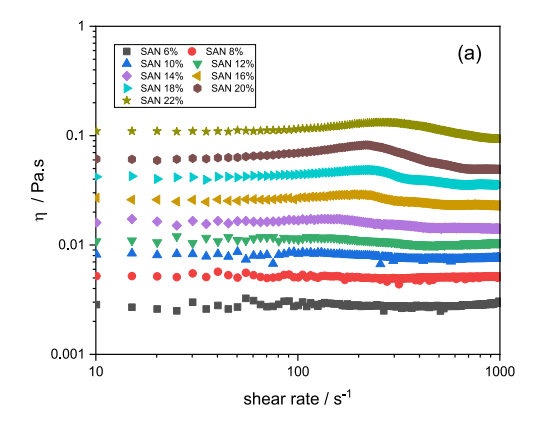
Fig. 6. Time vs. conversion curve (at $T=50\,^{\circ}$ C), for FTIR data (red line) and calorimetry data (blue line). Variation of the apparent activation energy (E_{α}) with α (green diamond).

concentrations. As shown in Fig. 7a, the viscosity of the SAN solution globally increases as a function of the polymer concentration. The low concentrated solutions have a Newtonian behavior at low shear $10-100 \, \rm s^{-1}$. A non-Newtonian behavior appears for a concentration higher than

10 % w/v and a shear rate $> 100 \text{ s}^{-1}$. An increase of the concentration entails the formation of entanglements among the polymer chains and it leads to a reduced mobility marked by a higher viscosity and a shearthinning behavior [47].

The Newtonian viscosity (η_0) was plotted as function of the polymer concentration. As displayed in Fig. 7b, two characteristic variations were observed for η_0 as a function of concentration. The η_0 changes follow a power-law behavior: exponent around 2 for concentration between 6 and 14 %, and exponent around 5 for concentration between 16 and 22 %, respectively. This result highlights the transition from a semidiluted to a semi-diluted entangled regime as previously reported for polystyrene solutions [46]. The transition is defined by the entanglement concentrations, c_e , which was estimated at around 15.5 %w/v. This change of regime is interesting as such change should also appear during the progress of dissolution in calorimetry or spectroscopy as the SAN concentration in MEK should progressively pass from 0 %w/v at the beginning of the dissolution to 20 % w/v (i.e. the maximum concentration when all the SAN is dissolved). Therefore, the changes associated with a semi-diluted to a semi-diluted entangled regime occurring at 15.5 %w/v could correspond to the point where a gel formation is observed in FTIR experiments. The gel layer would be caused by this progressive modification of the viscoelastic behavior, in particular in absence of shear, (i.e. no agitation in FTIR). This change in the regime is also consistent with the progressively larger energy barrier for SAN diffusion in the solvent obtained at the end of the calorimetric experiments (for $\alpha > 0.7$ in Fig. 3).

For recycling purposes, this change of regime is important for setting the initial conditions for dissolution of e.g. waste ABS. Indeed,



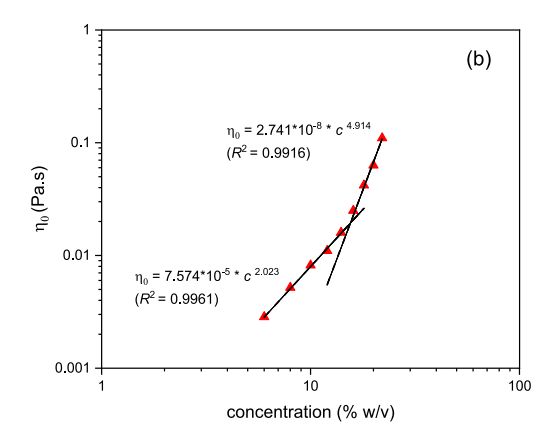


Fig. 7. (a) Viscosity versus shear rate at T = 30 °C for the different SAN concentration (6, 8, 10, 12, 14, 16, 18, 20, 22 %w/v); (b) Newtonian viscosity (red triangle), fixed at 10 s⁻¹, versus concentration at 30 °C, and power law fitting (dash black line).

depending on the initial solvent ratio, it might end up with a concentration of SAN in MEK that could be above or below this threshold of 15.5 %w/v. Being in the semi-diluted regime (i.e. concentration below 15.5 %) would be helpful to ensure that the solution can be relatively easily pumped from the reactor and transferred to filtration devices for removing the non-dissolved contents (i.e. polybutadiene rubber particles, additives, colorants, etc.) from the SAN solution. On the contrary, higher concentrations will favor the formation of gel layer as observed for instance in the FTIR measurement (20 %w/v).

The variation of the storage modulus (G') and the loss modulus (G'') as a function of angular frequency is shown in Fig. 8. A similar trend is observed for the four concentrations tested (8, 12, 18, and 22 % w/v). In the low frequency region, a liquid-like behavior is observed (G' < G''), whereas at higher ω , G' surpasses G'' rather corresponding to a solid-like behavior. The angular frequency at which the moduli G' and G'' crossover is denoted as ω_{Cross} . The relaxation time, t_R , is calculated as the reciprocal of the angular frequency ω_{Cross} .

$$t_{R} = \frac{1}{\omega_{\text{cross}}} \tag{17}$$

 t_R is the longest relaxation time and it represents the time taken by the polymer chains to disentangle.

As observed in Fig. 8, t_R decreases exponentially with increasing the concentration. A similar trend was already reported for polyacrylonitrile solutions in dimethylformamide [48].

The rheological behaviour of the system can be in part described by the Maxwell model over a frequency range. According to the Maxwell model, the storage modulus (G'), and the loss modulus (G'') are given by the following equations:

$$G'(\omega) = \frac{G_0(\omega t_R)^2}{1 + (\omega t_R)^2} \tag{18}$$

$$G''(\omega) = \frac{G_0 \omega t_R}{1 + (\omega t_R)^2} \tag{19}$$

$$\eta_0 = G_0 t_R \tag{20}$$

 G_0 is the plateau modulus, and it corresponds to the high-frequency G' plateau.

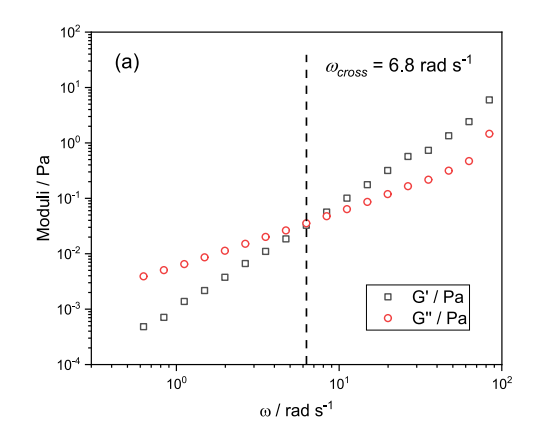
As shown in Fig. 9, it is interesting to note that for the angular frequency range from 0.01 to 200 rad.s⁻¹ both moduli increase with the angular frequency without reaching the maximum value of the plateau (G_0) as expected by the model.

5. Conclusion

Based on the HSP, MEK has been selected as suitable solvent for the SAN dissolution. This paper correlates the in-situ dissolution of SAN in MEK by correlating data obtained from calorimetry and FTIR spectroscopy. More insights were given on the thermodynamic and kinetic features of this dissolution. From a thermodynamic standpoint, the major enthalpic contribution in the dissolution comes from the enthalpic relaxation to pass from the glassy state to the rubbery state ($\Delta H_{transition}$) since, in comparison, the ΔH_{mixing} was much lower. From a kinetic standpoint, the dissolution is mainly governed by a single step process with an increase of the E_{α} at high conversion values corresponding to a control by diffusion. In-situ dissolution with ATR-FTIR spectroscopy allows to highlight that the dissolution proceeds quite fast with the appearance of the first SAN chains only two minutes after the beginning of the experiment. The band intensity increased until a plateau which corresponds with a gel layer formation. From the correlation between the results obtained from calorimetry and ATR-FTIR spectroscopy, we propose that the increase of the E_{α} at the end of the dissolution process could be associated to the diffusion of the SAN chains in the global volume of solution. Viscosity measurements on SAN solutions in MEK allowed to determine a transition between a semi-diluted and a semidiluted entangled regime at about 15.5 %w/v. Moreover, frequency sweep experiments pointed out a linear variation of the G', and G''moduli function of the frequency which deviates from the Maxwell model after the crossing point (G' = G''). Overall, this work paves the way to further investigations on plastic dissolution for physical recycling purpose. It might be that the enthalpic contribution, the activation barrier, and the viscosity regime might vary from a solvent to another. In the proper choice of solvent, these complementary features might guide the solvent selection. Moreover, the understanding of the temperaturedependance of such process both from a thermodynamic and kinetic standpoint is crucial for the design of the experiments and to foresee the upscaling of the process.

CRediT authorship contribution statement

Giuseppe Melilli: Writing – original draft, Methodology, Investigation, Formal analysis, Data curation. Sandra Litwin: Writing – original draft, Methodology, Investigation, Formal analysis, Data curation. Luc Vincent: Validation, Supervision, Methodology, Investigation, Formal analysis, Data curation. Nicolas Sbirrazzuoli: Writing – original draft, Validation, Supervision, Software, Methodology, Investigation, Data curation. Mark C.P. Roelands: Writing – review & editing, Validation, Funding acquisition, Conceptualization. Jan Cornelis van der Waal: Writing – review & editing, Methodology, Funding acquisition, Conceptualization. Ruud Cuypers: Writing – review & editing,



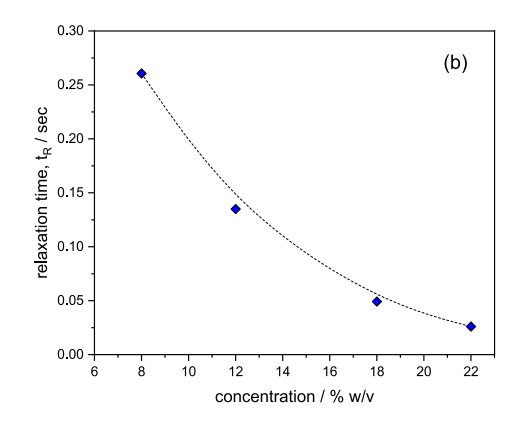
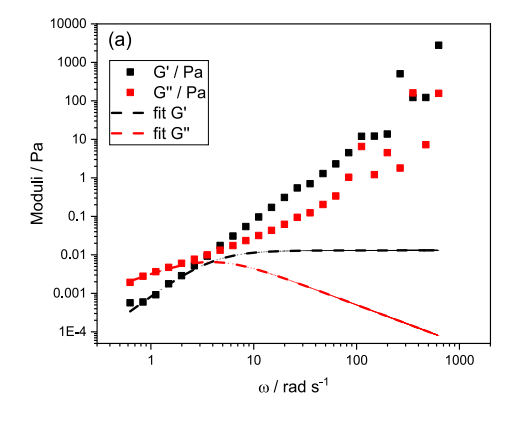
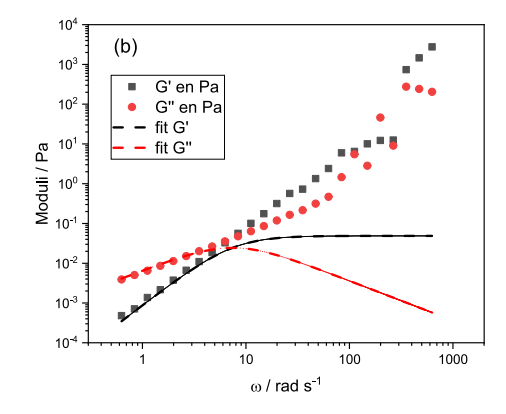
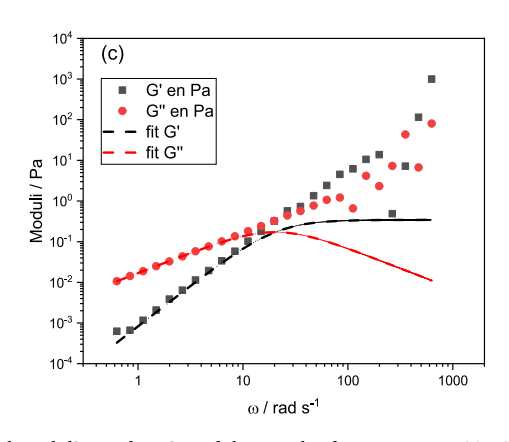


Fig. 8. (a) Example of a frequency sweep for SAN/MEK solution (concentration 12 %); (b) relaxation time (t_R) (filled blue diamond) versus concentration (8, 12, 18, 22 %w/v).







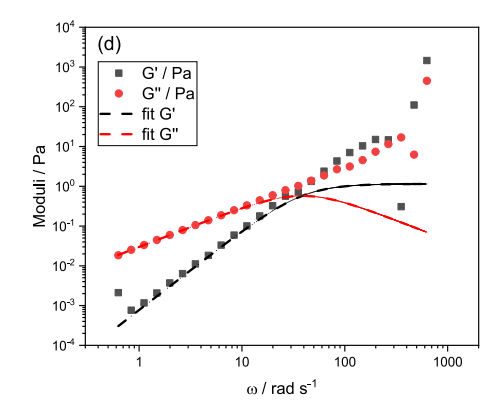


Fig. 9. Rheological moduli as a function of the angular frequency ω at 30 °C: concentration 8 % (a), 12 % (b), 18 % (c), and 22 % (d). Curves were fitted to the Maxwell model, (Eqs. (18) and (19)).

Validation, Project administration, Conceptualization. **Nathanael Guigo:** Writing – review & editing, Validation, Supervision, Project administration, Investigation, Funding acquisition, Conceptualization.

Funding

European Commission, grant no. 101058636.

Declaration of competing interest

The authors declare the following financial interests/personal relationships which may be considered as potential competing interests: Nathanael Guigo reports financial support was provided by Horizon Europe. If there are other authors, they declare that they have no known competing financial interests or personal relationships that could have appeared to influence the work reported in this paper.

Acknowledgements

The authors express their gratitude to the European Health and Digital Executive Agency (HADEA) under the power delegated by the European Commission for its support of the project ABSolEU — 'Paving the way for an ABS recycling revolution in the EU'.

Appendix A. Supplementary data

Supplementary data to this article can be found online at https://doi.org/10.1016/j.molliq.2024.126336.

Data availability

Data will be made available on request.

References

- M. Bachmann, C. Zibunas, J. Hartmann, V. Tulus, S. Suh, G. Guillén-Gosálbez, A. Bardow, Towards circular plastics within planetary boundaries, Nat. Sustain. 6 (5) (2023) 599–610, https://doi.org/10.1038/s41893-022-01054-9.
- [2] C.M. Rochman, M.A. Browne, B.S. Halpern, B.T. Hentschel, E. Hoh, H. K. Karapanagioti, L.M. Rios-Mendoza, H. Takada, S. Teh, R.C. Thompson, Classify plastic waste as hazardous, Nature 494 (7436) (2013) 169–171, https://doi.org/10.1038/494169a.
- [3] Solutions for plastic pollution, Nat. Geosci. 16(8) (2023) 655–655. doi: 10.1038/ s41561-023-01255-7.
- [4] A.R. Rahimi, J.M. Garciá, Chemical recycling of waste plastics for new materials production, Nat. Rev. Chem. 1 (6) (2017) 1–11, https://doi.org/10.1038/s41570-017.0046
- [5] Acrylonitrile Butadiene Styrene (ABS) Market Size is Predicted to reach USD 46.88 Billion by 2027, Says Brandessence Market Research, (n.d.). https://www.prnewswire.com/news-releases/acrylonitrile-butadiene-styrene-abs-market-size-is-predicted-to-reach-usd-46-88-billion-by-2027-says-brandessence-market-research-301304939.html (accessed September 21, 2023).
- [6] D. Deshmukh, H. Kulkarni, D.S. Srivats, S. Bhanushali, A.P. More, Polym. Bull. 81 (2024) 11361–11398, https://doi.org/10.1007/s00289-024-05269-y.
- [7] X. Liu, H. Bertilsson, Recycling of ABS and ABS/PC blends, J. Appl. Polym. Sci. 74 (1999) 510–515, https://doi.org/10.1002/(SICI)1097-4628(19991017)74:3.
- [8] K. Ragaert, L. Delva, K. Van Geem, Mechanical and chemical recycling of solid plastic waste, Waste Manag. 69 (2017) 24–58, https://doi.org/10.1016/J. WASMAN 2017 07 044
- [9] Y.B. Zhao, X.D. Lv, H.G. Ni, Solvent-based separation and recycling of waste plastics: a review, Chemosphere 209 (2018) 707–720, https://doi.org/10.1016/J. CHEMOSPHERE.2018.06.095.
- [10] A. Arostegui, M. Sarrionandia, J. Aurrekoetxea, I. Urrutibeascoa, Effect of dissolution-based recycling on the degradation and the mechanical properties of acrylonitrile-butadiene-styrene copolymer, Polym. Degrad. Stab. 91 (2006) 2768–2774, https://doi.org/10.1016/J.POLYMDEGRADSTAB.2006.03.019.

- [11] T. Lu, W.T. Chen, Material recycling of Acrylonitrile Butadiene Styrene (ABS) from toy waste using density separation and safer solvents, Resour. Conserv. Recycl. 197 (2023) 107090, https://doi.org/10.1016/J.RESCONREC.2023.107090.
- [12] G.S. Weeden, N.H. Šoepriatna, N.H.L. Wang, Method for efficient recovery of high-purity polycarbonates from electronic waste, Environ. Sci. Tech. 49 (2015) 2425–2433, https://doi.org/10.1021/ES5055786/SUPPL_FILE/ES5055786_SI_001_PDE
- [13] L. Wang, Y. Liu, H. Lu, Z. Huang, Recycling of phosphorus-containing plastic based on the dual effects of switchable hydrophilicity solvents, Chemosphere 259 (2020) 127402, https://doi.org/10.1016/j.chemosphere.2020.127402.
- [14] D. Arends, M. Schlummer, A. Mäurer, Removal of inorganic colour pigments from acrylonitrile butadiene styrene by dissolution-based recycling, J. Mater. Cycles Waste Manag. 14 (2012) 85–93, https://doi.org/10.1007/s10163-012-0041-5.
- [15] C.M. Hansen, Hansen Solubility Parameters: A User's Handbook, Second Edition -2nd, CRC Press, Boca Raton, 2007.
- [16] I. Tsampanakis, A.O. White, The mechanics of forming ideal polymer–solvent combinations for open-loop chemical recycling of solvents and plastics, Polymers (Basel) 14 (2022) 112, https://doi.org/10.3390/POLYM14010112/S1.
- [17] B.A. Miller-Chou, J.L. Koenig, A review of polymer dissolution, Prog. Polym. Sci. 28 (2003) 1223–1270, https://doi.org/10.1016/S0079-6700(03)00045-5.
- [18] J.S. Papanu, D.W. Hess, A.T. Bell, D.S. Soane, In situ ellipsometry to monitor swelling and dissolution of thin polymer films, J. Electrochem. Soc. 136 (1989) 1195–1200, https://doi.org/10.1149/1.2096852/XML.
- [19] I. Devotta, M.V. Badiger, P.R. Rajamohanan, S. Ganapathy, R.A. Mashelkar, Unusual retardation and enhancement in polymer dissolution: Role of disengagement dynamics, Chem. Eng. Sci. 50 (1995) 2557–2569, https://doi.org/ 10.1016/0009-2509(95)00103-C.
- [20] J.M. Hughes, D. Aherne, J.N. Coleman, Generalizing solubility parameter theory to apply to one- and two-dimensional solutes and to incorporate dipolar interactions, J. Appl. Polym. Sci. 127 (2013) 4483–4491, https://doi.org/10.1002/APP.38051.
- [21] T. Lindvig, M.L. Michelsen, G.M. Kontogeorgis, A Flory-Huggins model based on the Hansen solubility parameters, Fluid Phase Equilib. 203 (2002) 247–260, https://doi.org/10.1016/S0378-3812(02)00184-X.
- [22] S. Vyazovkin, A.K. Burnham, J.M. Criado, L.A. Pérez-Maqueda, C. Popescu, N. Sbirrazzuoli, ICTAC Kinetics Committee recommendations for performing kinetic computations on thermal analysis data, Thermochim. Acta 520 (2011) 1–19, https://doi.org/10.1016/J.TCA.2011.03.034.
- [23] S. Vyazovkin, Isoconversional Kinetics of Thermally Stimulated Processes, I, Springer, 2015.
- [24] S. Vyazovkin, A.K. Burnham, L. Favergeon, N. Koga, E. Moukhina, L.A. Pérez-Maqueda, N. Sbirrazzuoli, ICTAC kinetics committee recommendations for analysis of multi-step kinetics, Thermochim. Acta 689 (2020) 178597, https://doi.org/10.1016/J.TCA.2020.178597.
- [25] G. Melilli, N. Guigo, T. Robert, N. Sbirrazzuoli, Radical oxidation of itaconic acidderived unsaturated polyesters under thermal curing conditions, Macromolecules 55 (2022) 9011–9021, https://doi.org/10.1021/ACS.MACROMOL.2C01682/ SUPPL FILE/MA2C01682 SI 001.PDF.
- [26] S. Vyazovkin, Isoconversional methods: the many uses of variable activation energy, Thermochim. Acta 733 (2024) 179701, https://doi.org/10.1016/j. tca 2024 179701
- [27] N. Sbirrazzuoli, Interpretation and physical meaning of kinetic parameters obtained from isoconversional kinetic analysis of polymers, Polymers 12 (2020) 1280, https://doi.org/10.3390/POLYM12061280
- [28] H.L. Friedman, Kinetics of thermal degradation of char-forming plastics from thermogravimetry. application to a phenolic plastic, J. Polym. Sci., Part C: Polym. Symp. 6 (1964) 183–195, https://doi.org/10.1002/polc.5070060121.
- [29] S. Vyazovkin, Evaluation of activation energy of thermally stimulated solid-state reactions under arbitrary variation of temperature, J. Comput. Chem. 18 (1997) 393–402, https://doi.org/10.1002/(SICI)1096-987X(199702)18:3.
- [30] S. Vyazovkin, Modification of the integral isoconversional method to account for variation in the activation energy, J. Comput. Chem. 22 (2001) 178–183, https:// doi.org/10.1002/1096-987X.

- [31] N. Sbirrazzuoli, Determination of pre-exponential factors and of the mathematical functions f(α) or G(α) that describe the reaction mechanism in a model-free way, Thermochim. Acta 564 (2013) 59–69, https://doi.org/10.1016/J. TCA.2013.04.015.
- [32] N. Sbirrazzuoli, Advanced isoconversional kinetic analysis for the elucidation of complex reaction mechanisms: a new method for the identification of rate-limiting steps, Molecules 24 (2019) 1683, https://doi.org/10.3390/molecules24091683.
- [33] N. Sbirrazzuoli, Determination of pre-exponential factor and reaction mechanism in a model-free way, Thermochim. Acta 691 (2020) 178707, https://doi.org/ 10.1016/J.TCA.2020.178707.
- [34] S. Vyazovkin, N. Sbirrazzuoli, Isoconversional kinetic analysis of thermally stimulated processes in polymers, Macromol. Rapid Commun. 27 (2006) 1515–1532, https://doi.org/10.1002/marc.200600404.
- [35] N. Sbirrazzuoli, Kinetic analysis of complex chemical reactions by coupling model-free and model-fitting analysis, Thermochim. Acta 719 (2023) 179416, https://doi.org/10.1016/J.TCA.2022.179416.
- [36] S. Zhang, F.X. Li, J. Yong Yu, Y. Lo Hsieh, Dissolution behaviour and solubility of cellulose in NaOH complex solution, Carbohydr. Polym. 81 (2010) 668–674, https://doi.org/10.1016/J.CARBPOL.2010.03.029.
- [37] A.M. Basedow, K.H. Ebert, W. Feigenbutz, Polymer-solvent interactions: Dextrans in water and DMSO, Die Makromolekulare Chem. 181 (1980) 1071–1080, https:// doi.org/10.1002/MACP.1980.021810511.
- [39] A.P. Safronov, T.V. Terziyan, The enthalpy of dilution as a direct characteristic of the energy spectrum of intermolecular interaction in polymer solutions and gels, Polym. Sci. – Ser. A 50 (2008) 733–742, https://doi.org/10.1134/ S0965545X0807002X/METRICS.
- [40] R.J. Pace, A. Datyner, Statistical mechanical model for diffusion of simple penetrants in polymers. III. Applications—vinyl and related polymers, J. Polym. Sci. Polym. Phys. Ed. 17 (1979) 465–476, https://doi.org/10.1002/ pol.1979.180170311.
- [41] R. Watanabe, A. Oishi, S. Nakamura, H. Hagihara, H. Shinzawa, Real-time monitoring of the thermooxidative degradation behavior of poly(acrylonitrilebutadiene-styrene) using isothermal in-situ Fourier transform infrared spectroscopy combined with principal component analysis, Polymer (Guildf) 283 (2023) 126243, https://doi.org/10.1016/J.POLYMER.2023.126243.
- [42] A. Agirre, M. Aguirre, J.R. Leiza, Characterization of grafting properties of ABS latexes: ATR-FTIR vs NMR spectroscopy, Polymer (Guildf) 253 (2022) 124997, https://doi.org/10.1016/J.POLYMER.2022.124997.
- [43] Y. Eom, H. Ju, Y. Park, D.W. Chae, Y.M. Jung, B.C. Kim, H.G. Chae, Effect of dissolution pathways of polyacrylonitrile on the solution homogeneity: thermodynamic- or kinetic-controlled dissolution, Polymer (Guildf) 205 (2020) 122697. https://doi.org/10.1016/J.POLYMER.2020.122697.
- [44] S. Vyazovkin, N. Sbirrazzuoli, Mechanism and kinetics of epoxy-amine cure studied by differential scanning calorimetry, Macromolecules 29 (1996) 1867–1873, https://doi.org/10.1021/MA951162W.
- [45] N. Sbirrazzuoli, S. Vyazovkin, A. Mititelu, C. Sladic, L. Vincent, A study of epoxyamine cure kinetics by combining isoconversional analysis with temperature modulated DSC and dynamic rheometry, Macromol. Chem. Phys. 204 (2003) 1815–1821, https://doi.org/10.1002/MACP.200350051.
- [46] Y. Eom, B.C. Kim, Solubility parameter-based analysis of polyacrylonitrile solutions in N, N-dimethyl formamide and dimethyl sulfoxide, Polymer (Guildf) 55 (2014) 2570–2577, https://doi.org/10.1016/J.POLYMER.2014.03.047.
- [47] R. Kol, P. Nachtergaele, T. De Somer, D.R. D'Hooge, D.S. Achilias, S. De Meester, Toward more universal prediction of polymer solution viscosity for solvent-based recycling, Ind. Eng. Chem. Res. 61 (2022) 10999–11011, https://doi.org/10.1021/ ACS_IECR_2C01487/ASSET/IMAGES/LARGE/IE2C01487 0009_JPEG.
- [48] C.E. Brunchi, M. Bercea, S. Morariu, Viscometric and rheological study of polyacrylonitrile solutions, E-Polymers 9 (2009), https://doi.org/10.1515/ EPOLY.2009.9.1.803/MACHINERFADABLECITATION/RIS.